Inorg. Chem. **2005**, *44*, 7876–7885

Pyridine-Substituted Oligopeptides as Scaffolds for the Assembly of Multimetallic Complexes: Variation of Chain Length

Kristi Ohr, Brian P. Gilmartin, and Mary Elizabeth Williams*

The Pennsylvania State University, Department of Chemistry, 104 Chemistry Building, University Park, Pennsylvania 16802

Received May 13, 2005

This paper presents the synthesis and characterization of pyridine-substituted artificial oligopeptides with an aminoethylglycine backbone of varying length, which are designed to act as scaffolds for the self-assembly of multimetallic structures. The identities and purities of the oligopeptides are confirmed with mass spectrometry, ^{1}H NMR, HPLC, and pH titrations. The acid dissociation constants for the oligopeptides were determined and were found to decrease with increasing pyridine units. Titrations of the oligopeptides with Cu(II) and Pt(II) complexes containing the tridentate ligands 2,2′:6′,2″-terpyridine and pyridine 2,6-dicarboxylic acid were monitored using UV–visible absorption spectroscopy and showed stoichiometric binding based on the number of pyridines on the peptide strand. Metal titrations performed using an analogous oligopeptide with methyl substituents (in place of the pyridine ligands) showed very weak or no binding. In the case of the oligopeptides containing bound Pt(terpyridine)$^{2+}$ complexes, cyclic voltammetry reveals two sequential one-electron reductions at formal potentials that do not vary as a function of oligopeptide length. The measured diffusion coefficients were measured with chronoamperometry and were found to decrease with increasing oliopeptide length.

Introduction

The molecular recognition by complementary sequences of DNA provides a unique and challenging benchmark, in terms of both binding specificity and affinity, for the creation of analogous supramolecular inorganic materials. In the initial steps toward the creation of synthetic analogues, the synthesis and stabilities of peptide nucleic acids (PNAs) in which one nucleic acid is replaced with a ligand capable of metal complexation,[1] similar to studies done with DNA,[2] have recently been reported. However, these studies primarily rely on *hydrogen bonding* to achieve molecular recognition and focus on the enhanced stabilities of duplexes that result from the metal complexation of the single incorporated ligand-for-nucleotide substitution. Alternatively, if duplex (and higher order) formation is based solely on metal−ligand complexation, this would provide a more robust linkage than hydrogen bonding. This strategy has been used to mimic the structure of DNA (and RNA) by incorporation of the ligands onto the anionic sugar phosphoester backbone.[3] While PNA is a structural analogue of DNA,[4] the amide linkages are charge neutral so that there are no interstrand electrostatic repulsive forces. Complementary PNA−DNA duplexes in fact have greater binding affinity than DNA−DNA duplexes.[4a,5] Adaptation of the metal-coordination strategy to the aminoethylglycine (aeg) backbone should therefore provide an even more tightly bound duplex structure. Despite the much greater stability that would be imparted by such a binding motif, there have been no examples in the literature that utilize only metal complexation as the basis for molecular recognition in oligopeptides.

* To whom correspondence should be addressed. E-mail: mbw@chem.psu.edu.

(1) (a) Popescu, D.; Parolin, T. J.; Achim, C. *J. Am. Chem. Soc.* **2003**, *125*, 6354−6355. (b) Mokhir, A.; Stiebing, R.; Kraemer, R. *Bioorg. Med. Chem. Lett.* **2003**, *13*, 1399−1401.

(2) (a) Meggers, E.; Holland, P. L.; Tolman, W. B.; Romesberg, F. E.; Schultz, P. G. *J. Am. Chem. Soc.* **2000**, *122*, 10714−10715. (b) Weizman, H.; Tor, Y. *J. Am. Chem. Soc*. **2001**, *123*, 3375−3376. (c) Artwell, S.; Meggers, E.; Spraggon, G.; Schultz, P. G. *J. Am. Chem. Soc*. **2001**, *123*, 12364−12367. (d) Tanaka, K.; Yamada, Y.; Shionoya, M. *J. Am. Chem. Soc.* **2002**, *124*, 8802−8803. (e) Tanaka, K.; Tengeiji, A.; Kato, T.; Toyama, N.; Shiro, M.; Shionoya, M. *J. Am. Chem. Soc*. **2002**, *124*, 12494−12498.

(3) (a) Tanaka, K.; Tengeiji, A.; Kato, T.; Toyama, N.; Shionoya, M. *Science* **2003**, *299*, 1212−1213. (b) Shionoya, M. *Macromol. Symp*. **2004**, *209*, 41−50.

(4) (a) Hyrup, B.; Nielsen, P. E. *Bioorg. Med. Chem.* **1996**, *4*, 5−23. (b) Nielsen, P. E.; Egholm, M.; Buchardt, O. *Bioconjugate Chem.* **1994**, *5*, 3−7.

(5) Orum, H.; Nielsen, P. E.; Jorgensen, M.; Larsson, C.; Stanley, C.; Koch, T. *Biotechniques* **1995**, *19*, 472−480.

10.1021/ic050769i CCC: $30.25
Published on Web 09/23/2005

We recently reported the synthesis of pyridine-substituted hexapeptides and bipyridine-substituted tripeptides and demonstrated that these molecules can be used to bind stoichiometric amounts of metal ions.[6] In the case of the bipyridine tripeptide, complexation of Cu^{2+} and Fe^{2+} created interstrand cross-links that led to the formation of duplex structures based solely on metal coordination.[6] This paper builds on that initial work by examining the structural and functional properties of the single-strand pyridine oligopeptides as a function of the number of attached pyridyl ligands on a series of peptide lengths. Spectrophotometric titrations using Pt(II) and Cu(II) complexes of two tridentate ligands, 2,2′:6′,2″-terpyridine (tpy) and pyridine 2,6-dicarboxylic acid (pda), are employed to quantitatively determine the reactivity of this family of pyridine-substituted oligopeptides toward metal complexation. These experiments demonstrate synthetic control over a wide range of multimetallic structures. We investigate the degree of interaction of the metal ions with the peptide backbone in analogous titrations with an acetyl-substituted derivative of the oligopeptide. In the case of the $[Pt(tpy)]^{2+}$ oligopeptide complexes, we present electrochemical characterization of their solution phase transport and electron-transfer properties to further understand their solution structures and show their unique properties.

Experimental Section

Chemicals. All materials were purchased from Acros and were used as received unless otherwise noted. Water was obtained from a Nanopure water system (Barnstead, 18.2 MΩ). *N*,*N*-Dimethylformamide (DMF) and diisopropylethylamine (DIPEA) were purified by distillation under N_2 from CaH_2. Tetrabutylammonium hexafluorophosphate (TBAH) was recrystallized from ethyl acetate (EtOAc) three times and dried under vacuum prior to use. Ferrocene (Fc) was purified by sublimation.

Instrumentation and Analysis. Automated peptide synthesis was performed on a flow-through synthesizer (Applied Biosystems Pioneer). Preparatory- and analytical-scale reverse-phase high performance liquid chromatographies (HPLC) were performed with a Varian system equipped with two quaternary pumps (Model 210), an autosampler (Model 410), a UV−vis detector (Model 320), a fraction collector (Model 701), and C-18 columns. Oligomer elution was monitored at the pyridine absorbance at 254 nm.

Molecular structures were calculated using Hyperchem 6.0 using molecular mechanics (MM+) with atomic-charge-based electrostatic repulsions and a Polack−Ribiere conjugate gradient to a minimum energy gradient of 0.01 kcal/mol.

The UV−visible absorption spectra were obtained with a double-beam spectrophotometer (Varian, Cary 500). Positive-ion electrospray mass spectrometry (ESI+) was performed at the Penn State Mass Spectrometry Facility using a Mariner mass spectrometer (Perseptive Biosystems.) ^{1}H NMR spectra were collected on a 300 MHz spectrophotometer (Bruker).

All electrochemical measurements were obtained using a CH Instruments potentiostat (Model 660) with a 0.31 cm diameter glassy carbon working and Pt wire counter electrodes with a Ag/Ag^+ reference electrode. Solutions were prepared from distilled DMF containing 0.2 M TBAH supporting electrolyte. The solutions were prepared, stored, and analyzed in an N_2 saturated environment. After voltammograms were obtained, Fc was added as an internal potential reference to convert to the SCE scale.[7] Choronoamperometric measurements were corrected for background currents by subtraction of the current transients obtained from potential steps of equal magnitude applied in solutions containing solely supporting electrolyte.

Synthesis. ***Caution:*** *Perchlorate salts are potentially explosive and should be handled with care.* The synthesis of aqua(pyridine-2,6-dicarboxylato)copper(II)[8] (i.e., [Cu(pda)]), aqua(2,2′:6′,2″-terpyridine)copper(II) diperchlorate[9] (i.e., $[Cu(tpy)]^{2+}$), aqua(pyridine-2,6-dicarboxylato)platinum(II)[10] (i.e., [Pt(pda)]), and *N*-[2-(Fmoc-aminoethyl]glycinate *tert*-butylester hydrochloride[11] (i.e., Fmoc-aeg-O*t*Bu·HCl) have been reported elsewhere. The synthesis of aqua(2,2′:6′,2″-terpyridine-*N*,*N*′,*N*″)platinum(II) diperchlorate (i.e., $[Pt(tpy)]^{2+}$) was adapted from a literature procedure using $AgClO_4$ instead of $AgBF_4$.[12] The pyridine-substituted aeg monomer (Fmoc-aeg(py)-OH·HCl) was synthesized as reported previously.[6]

Fmoc-aeg(Ac)-OH (Acetyl monomer). Glacial acetic acid (1.00 mL, 0.0174 mol), 1-(3-dimethylaminopropyl)-3-ethylcarbodiimide hydrochloride (EDC, 3.34 g, 0.0174 mol), 1-hydroxybenzotriazole hydrate (HOBt, 2.35 g, 0.0174 mol), Fmoc-aeg-O*t*Bu·HCl (6.03 g, 0.0139 mol), and DIPEA (5.46 mL, 0.0313 mol) were combined in 200 mL of CH_2Cl_2 and stirred for 24 h under N_2. The solution was washed with H_2O (5 × 100 mL) and evaporated to dryness. The resulting oil was chromatographed on silica gel with 25 acetone/75 CH_2Cl_2, and the *t*-Bu-protected product was isolated as the major band. The *t*-Bu group was cleaved by strirring in 100 mL of 25% trifluoroacetic acid (TFA) in CH_2Cl_2 for 30 min and evaporating to dryness. The pure product was precipitated as a white solid from cold CH_2Cl_2 by addition of Et_2O and was collected by vacuum filtration. Yield: 1.09 g (21%) (^{1}H NMR, 300 MHz, CD_3Cl): 2.05 (d, 3H); 3.25 (m, 2H); 3.40 (m, 2H); 3.88 (d, 2H); 4.11 (m, 1H); 4.31 (m, 2H); 5.51,5.88 (m, 1H); 7.25 (t, 2H); 7.35 (t, 2H); 7.55 (d, 2H), 7.69 (d, 2H)

Pyridine Oligomers (1, 4, 5, 6, 10). The oligomers were prepared from the pyridine monomer (Fmoc-aeg(py)-OH·HCl) as described previously.[6] Briefly, the oligopeptides were prepared via automated solid-phase peptide synthesis in DMF using an Fmoc protection scheme at a 0.1 mmol scale using Fmoc-PAL-PEG-PS resin (Applied Biosystems). Deprotection was performed for 5 min with 20% piperidine in DMF. Couplings were carried out using a 4-fold molar excess of oligomers for 30 min with separate solutions of 0.5 M diisopropylcarbodiimide (DIPCDI) and 0.5 M DIPEA. Capping steps were performed after each coupling using 0.5 M benzoic anhydride and 0.5 M DIPEA in DMF for 5 min.

Oligopeptides were cleaved from the resin using 2.5% triisopropylsilane and 2.5% water in TFA. Upon filtration into cold ether, the peptides and deletions were obtained as white to off-white precipitates. These were collected by centrifugation and washed with ether (3 × 10 mL). The pure oligopeptides were obtained by

(6) Gilmartin, B. P.; Ohr, K.; McLaughlin, R. L.; Koerner, R.; Williams, M. E. *J. Am. Chem. Soc.* **2005**, *127*, 9546−9555.

(7) Bard, A. J.; Faulkner, L. R. *Electrochemical Methods, Fundamentals and Applications*, 2nd ed.; John Wiley and Sons: New York, 2001.

(8) Murtha, D. P.; Walton, R. A. *Inorg. Chim. Acta* **1974**, *8*, 279−284.

(9) Yamauchi, O.; Benno, H.; Nakahara, A. *Bull. Chem. Soc. Jpn.* **1973**, *46*, 3458−3462.

(10) Cattalini, L.; Chessa, G.; Marangoni, G.; Pitteri, B.; Celon, E. *Inorg. Chem.* **1989**, *28*, 1944−1947.

(11) Thompson, S. A.; Josey, J. A.; Cadilla, R.; Gaul, M. D.; Hassman, C. F.; Luzzio, M. J.; Pipe, A. J.; Reed, K. L.; Ricca, D. J.; Wiethe, R. W.; Noble, S. A. *Tetrahedron* **1995**, *51*, 6179−6194.

(12) (a) Clark, H. C.; Manzer, L. E. *J. Orgmet. Chem.* **1973**, *59*, 411−428. (b) McDermott, J. X.; White, J. F.; Whitesides, G. M. *J. Am. Chem. Soc.* **1976**, *98*, 6521−6528. (c) Lowe, G.; Vilaivan, T. *J. Chem. Res. (S)* **1996**, 386-387.

Table 1. Characterization Data for the Pyridyl Oligopeptides **1**, **4**, **5**, **6**, and **10**

	oligopeptide				
	1	**4**	**5**	**6**	**10**
yield (% yield)[a]	41 mg (29%)	45 mg (30%)	69 mg (37%)	92 mg (42%)	192 mg (55%)
purity[b]	99.1%	99.0%	99.8%	98.0%	99.3%
$(M + H)^+$ found (calcd)[c]	398.3 (398.2)	1056.6 (1056.5)	1274.5 (1274.6)	1493.8 (1493.7)	1186.7[d] (1186.6)[d]
titration equivalence point[e]	1.27	4.06	4.88	6.17	10.1
pK_A[f]	5.04	4.45	3.53	3.38	3.8

[a] Percent yield of the final, purified product based on the loading level of the resin. [b] Percentage purity of the product following separation by preparatory-scale HPLC, based on the area of the integrated peak on a subsequent analytical-scale HPLC injection. [c] Observed *m*/*z* peak in the positive-ion electrospray ionization mass spectrum versus the predicted value. [d] $(M + 2H)^{2+}$ peak. [e] Molar equivalence point (mol OH^-/mol oligopeptide) determined from the pH titration curve. [f] The acid dissociation constant, determined from the half-equivalence point of the pH titration curve.

Scheme 1. (A) Monomer Syntheses[a] and (B) Structures of the Pyridyl and Acetyl Oligomers

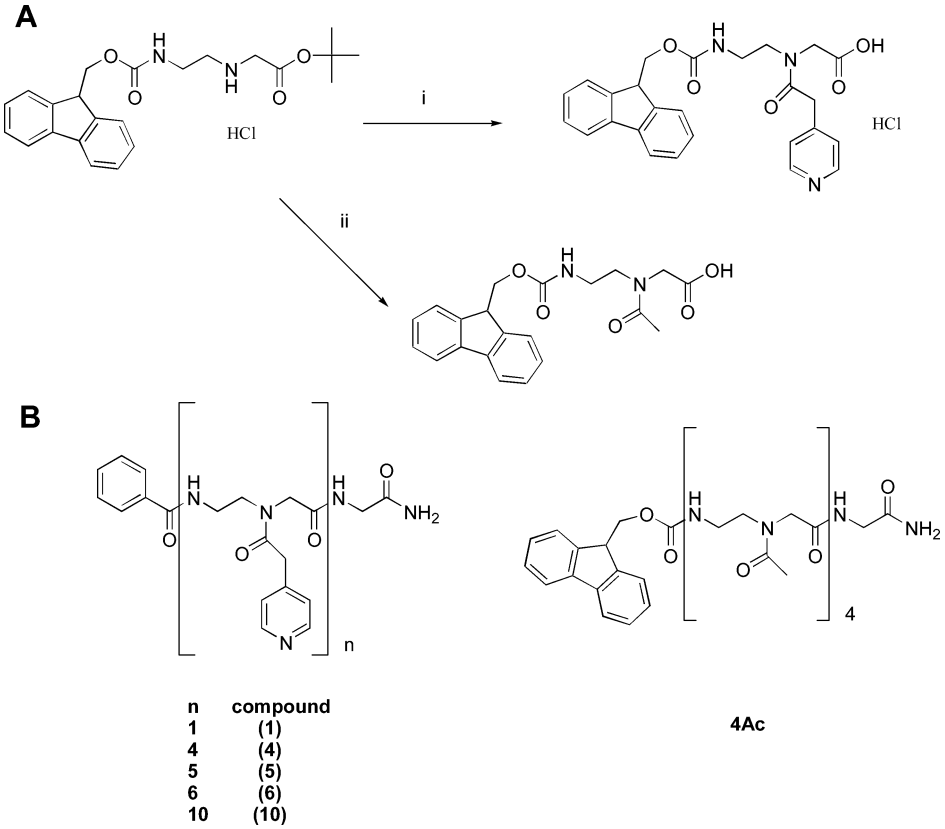

n	compound
1	(1)
4	(4)
5	(5)
6	(6)
10	(10)

[a] (i) 1. CH_2Cl_2, EDC, HOBt, DIPEA, 4-pyridylacetic acid hydrochloride; 2. 3 M HCl; (ii) 1. CH_2Cl_2, EDC, HOBt, DIPEA, glacial acetic acid; 2. TFA/CH_2Cl_2.

preparatory-scale reverse-phase HPLC by elution with a solvent gradient ramp of 5:95 to 15:85 (v/v of 0.1% TFA in acetonitrile/0.1% aqueous TFA) for 10 min with a total flow rate of 20 mL/min. In each case, the oligopeptide was found to be the major peak. The oligopeptides were isolated as white solids following flash evaporation and lyophilization. Yields are given in Table 1. Purity was assessed with analytical-scale HPLC by elution with a solvent gradient from 0.1% aqueous TFA to 0.1% TFA in acetonitrile (ramped over 100 min) and a flow rate of 1 mL/min. Only one peak was observed in the chromatogram in each case, and the percentage purity from these is given in Table 1. Identity of the oligopeptides was confirmed with ESI+ mass spectrometry, and the calculated and observed *m*/*z* are given in Table 1. Purity, identity, and dryness (following extensive lyophilization) were confirmed with ^{1}H NMR (see Supporting Information for example). (^{1}H NMR, 300 MHz, d_6-DMSO): Compound (**1**): 3.1−3.65 (m, 6H), 3.85 (d, 2H), 3.98 (s, 1H), 4.05 (s, 1H), 6.75−7.10 (s−s, 1H), 7.22 (m, 4H), 7.54 (m, 4H), 7.75−8.41 (m−m, 2H), 8.60 (t, 2H); Compound (**4**): 3.10−3.79 (m, 19H), 3.80−4.30 (m, 15H), 7.11 (s, 1H), 7.25 (s, 1H), 7.45 (m, 5H), 7.77 (m, 9H), 8.03 (m, 1H), 8.19−8.59 (m−m, 3H), 8.80 (m, 8H); Compound (**5**): 3.02−3.73 (m, 23H), 3.51−4.31 (m, 19H), 7.11 (s, 1H), 7.21 (s, 1H), 7.48 (m, 6H), 7.82 (m, 11H), 8.05 (m, 1H), 8.33 (m, 1H), 8.50 (m, 1H), 8.72 (m, 11H); Compound (**6**): 3.15−3.75 (m, 26H), 3.75−4.30 (m, 24H), 7.08 (s, 1H), 7.21 (s, 1H), 7.50 (m, 4H), 7.71 (m, 14H), 8.01 (m, 1H), 8.30 (m, 3H), 8.50 (m, 2H), 8.70 (m, 12H); Compound (**10**): 3.05−3.78 (m, 45H), 4.78−4.30 (m, 37H), 7.10 (s, 2H), 7.25 (s, 2H), 7.45 (m, 11H), 7.78 (m, 19H), 8.00 (m, 1H), 8.28 (m, 4H), 8.47 (m, 3H), 8.70 (m, 16H).

Acetyl Tetramer Synthesis (4Ac). The acetyl tetramer was prepared using analogous coupling steps by hand with the acetyl monomer (Fmoc-aeg(Ac)-OH) in Scheme 1. The tetramer was purified by preparatory-scale HPLC with a gradient elution of 20:80 to 50:50 (v/v 0.1% TFA in CH_3CN/0.1% TFA in H_2O) ramped

over 13 min with a total flow of 20 mL/min. The major peak was isolated and dried as above and determined to be the desired tetramer product using mass spectrometry and NMR. ESI+ mass spectrometry: Calcd, $(M + H)^+ = 865.42$; Found $(M + H)^+ = 865.5$ ^{1}H NMR (300 MHz, d_6-DMSO): 1.32 (m, 9H), 1.99 (m, 4H), 2.68 (m, 2H), 3.40 (m, 12H), 3.92 (m, 5H), 4.28 (m, 6H), 7.13 (m, 1H), 8.39 (m, 3H), 8.64 (m, 3H), 7.93 (m, 4H), 8.23 (m−m, 1H), 8.85 (m, 3H)

pH Titrations. Following lyophilization for up to 72 h, the dryness of the oligomers **1**, **4**, **5**, **6**, and **10** was confirmed by ^{1}H NMR; these were then weighed and dissolved in water to a total volume of 5.00 mL. The solutions were then titrated with 0.0994 ± 0.0001 M NaOH (standardized against potassium hydrogen phthalate, KHP), and the pH monitored with an electrode (Accumet, Fisher Scientific) calibrated versus standard buffers until the pH reached ∼11−12. The equivalence point was determined from the *x* intercept of the second derivative of the titration curve, and the pK_A as the pH value at half-equivalence; these are given in Table 1.

Addition Of Metal Complexes. Following lyophilization, solutions of **1**, **4**, **5**, **6**, and **10** were prepared in spectroscopic-grade MeOH and the pyridine concentrations were determined from a calibration curve generated for the pyridine monomer as described previously,[6] using $\epsilon = 5310\ M^{-1}\ cm^{-1}$ at 255 nm. The complexation of $[Pt(tpy)]^{2+}$, [Pt(pda)], [Cu(pda)], and $[Cu(tpy)]^{2+}$ with each of the oligomers was monitored by UV−visible absorption spectroscopy. Solutions of known concentration of [Cu(pda)] in MeOH, $[Cu(tpy)]^{2+}$ in 2.5% H_2O in MeOH, $[Pt(tpy)]^{2+}$ in 25% H_2O in MeOH, and [Pt(pda)] in H_2O were prepared. Typical concentrations for metals were ∼10 mM for the Cu compounds and 0.1 mM for the Pt species. For each experiment, the same metal complex solution was placed in the sample and reference cuvettes of a double-beam spectrophotometer. The oligomer solution was then added in 25 μL increments to the sample beam cuvette; an equivalent volume of solvent was added to the reference cell. In the case of the Cu complexes, solutions were stirred for a minimum of 5 min at room temperature for each iterative addition; the Pt solutions were stirred for 5 min at 50 °C and then 5 min at room temperature. The UV−visible absorbance difference spectrum was measured after each addition. Because the oligomer absorbance is similar in wavelength to the Pt complex, the difference spectra were manually corrected for this additional background absorbance.

The Cu-complexed oligopeptides were isolated as powders by precipitation upon addition of ether and dried for a minimum of 2 days under vacuum prior to structural analysis. $[Pt(tpy)]^{2+}$-containing oligomers were precipitated by the addition of saturated aqueous ammonium hexafluorophosphate (NH_4PF_6), washed with water, 2-propanol, and ether, and dried in a vacuum at 70 °C for 3 days prior to structural analysis and electrochemical characterization. (^{1}H NMR, 300 MHz, d_6-DMSO):

[Cu(pda)]-Containing Oligomers. (**1**): 3.18−4.30 (mm, 10H), 6.85−8.79 (mm, 9H); (**4**): 2.78−4.49 (mm, 34H), 6.59−8.35 (mm, 12H); (**5**): 2.82−4.40 (mm, 42H), 6.80−8.95 (mm, 13H); (**6**): 2.55−4.19 (mm, 50H), 6.68−8.73 (mm, 14H); (**10**): 2.62−4.30 (mm, 82H), 6.81−8.78 (mm, 18H).

$[Cu(tpy)]^{2+}$-Containing Oligomers. (**1**): 3.02−4.45 (mm, 10H), 6.49−8.20 (mm, 9H); (**4**): 2.90−4.38 (mm, 34H), 6.76−8.79 (mm, 12H); (**5**): 3.05−4.40 (mm, 42H), 6.91−8.90 (mm, 13H); (**6**): 2.90−4.35 (mm, 50H), 6.88−8.79 (mm, 14H); (**10**): 2.78−4.20 (mm, 82H), 6.87−8.79 (mm, 18H).

$[Pt(tpy)]^{2+}$-Containing Oligomers. (**1**): 3.40−3.89 (m, 6H), 4.05 (s, 1H), 4.15 (s, 1H), 4.20 (s, 1H), 4.35 (s, 1H), 7.20 (s, 1H), 8.46 (m, 3H), 8.88 (m, 5H), 8.97 (m, 2H), 8.29 (m, 1H), 8.65 (mm, 10H), 8.95 (m, 1H), 9.05 (m, 2H); (**4**): 2.85−3.50 (m, 18H), 3.50−4.20 (m, 16H), 6.61−7.82 (mm, 36H), 7.82−8.92 (mm, 36H); (**5**): 2.45−4.15 (mm, 42H), 7.15−7.92 (mm, 18H), 8.08−8.91 (mm, 60H); (**6**): 3.02−4.42 (mm, 50H), 7.11−8.10 (mm, 32H), 8.22−9.15 (mm, 72H); (**10**): 2.90−4.25 (mm, 82H), 6.93−7.89 (mm, 70H), 7.99−9.00 (mm, 98H).

Results and Discussion

Oligomer Characterization. The pyridine-substituted artificial oligopeptides were prepared via standard automated solid-phase peptide synthesis (SPPS) using an Fmoc protection scheme. The oligomer yields, based on the loading of the solid-phase support, range from 29 to 52% and are equal to or better than those for natural oligopeptides synthesized via SPPS. The oligomer identities were verified with electrospray ionization mass spectrometry, and the purities were assessed by slow-gradient-ramping analytical-scale HPLC after bulk purification (Table 1). Lyophilization of the peptides was continued until there was no evidence for the presence of solvent in the ^{1}H NMR spectrum (see Supporting Information). ^{1}H NMR data are qualitatively complicated due to the presence of rotamers; however, on the basis of the peak integrations, these confirm the identity and purity of the desired oligopeptide sequence.

The oligopeptides are isolated and purified in the presence of excess amounts of trifluoroacetic acid, so that the pyridyl units are fully protonated as their TFA salts. Because the oligomers are isolated as dry solids following lyophilization, their masses may be measured with reasonable accuracy (and used together with their molecular weights as TFA salts) to prepare solutions of known concentration. Protonated pyridines are weak acids that may be deprotonated by equivalent addition of a strong base, so that neutralization provides a means to accurately determine the amount of acidic pyridyl protons per oligomer. Thus, titrations are a tool for verification of the identity and relative purity of the oligomer, since significant amounts of impurities or an incorrect oligopeptide molecular weight (i.e., its identity) would cause a deviation in the predicted amount of base required. We therefore utilize pH titrations with NaOH to determine the identity and purity of the oligomers; a representative titration curve is shown in Figure 1A for the pyridyl hexapeptide **6**. For oligomers **1**, **4**, **5**, **6**, and **10**, the titration curves have a single inflection point that indicates the pH at which the concentrations of base and pyridyl acid are the same (i.e., the titration equivalence point). The existence of only one equivalence point for each oligomer indicates that all of the pyridines on the oligomer are simultaneously neutralized and therefore act *independently*. The equivalence points for oligomers **1**, **4**, **5**, **6**, and **10** are determined from the second derivative of their titration curves and are given in Table 1. These values agree well with those predicted on the basis of the length of the oligopeptides; the small errors in these values most likely arise from uncertainties associated with the oligopeptide concentration due to small amounts of water or salt that were not detectable by NMR. We find that there is a linear relationship between the equivalence point and the number of pyridyl ligands on each oligomer (determined separately)

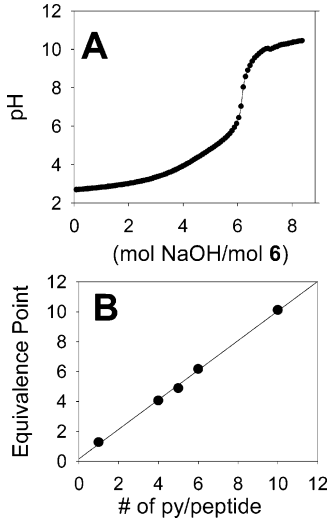

Figure 1. (A) Titration curve of the change in pH as a function of the amount of added 99.4 ± 0.1 mM NaOH to 12.0 μM oligomer **6**, plotted in terms of the relative molar quantities of base and oligomer **6** (■); (B) Plot of the equivalence point versus the number of pyridyl groups on each oligopeptide, with linear regression.

with a slope of 0.99 (Figure 1B). We therefore are able to utilize straightforward titrations to quickly assess oligopeptide synthesis products.

Further analysis of the titration curves allows comparison of the acid dissociation constants (pK_A, the pHs at their half-equivalence points) of the pyridine oligopeptides. The pK_A of the "unimer", **1**, which contains only a single pyridine ligand, is 5.04 and agrees with the known pK_A for pyridine, 5.23.[13] Table 1 indicates that the pK_A's of the oligopeptides generally *decrease* as the number of pyridyl monomers increase. This is likely a result of electrostatic repulsions between positively charged, protonated pyridines; as the chain lengthens, the larger number of cations increases the electrostatic force that pushes the pyridines farther apart. Similar observations have been reported for pyridine-containing polymers.[14] The lower pK_A's of longer oligopeptides suggest an increase in deprotonation efficiency or lower stability of the protonated oligopeptide. This is consistent with the observed changes in the equivalence points, where the pyridyl groups must be far enough apart to deprotonate independently. In the case of **10**, which deviates from this trend, the peptide may be long enough so that it can twist to decrease these repulsive forces, and therefore, the pK_A is slightly larger.

Reaction with Cu and Pt Complexes. The oligopeptides **1**, **4**, **5**, **6**, and **10** contain pyridyl groups that can also function as ligands in metal complexes. To examine the ability of the pyridine-containing oligopeptides to bind metals, we selected four metal complexes containing either Pt(II) or Cu(II) with one tridentate ligand, $[Cu(tpy)]^{2+}$, $[Pt(tpy)]^{2+}$, [Pt(pda)], and [Cu(pda)]. The Pt(II) and Cu(II) in each of these are known to prefer tetracoordinate geometries, so that in the presence of a monodentate pyridine ligand, each should bind in one-to-one fashion. This strategy allows us to confirm that the pyridyl ligands act independently during metal coordination, analogous to the neutralization titrations above, as shown in Scheme 2.

Formation of a metal−pyridine bond typically leads to the formation of an absorbance peak in the visible region of the spectrum, and we therefore monitored metal complexation using UV−visible absorption spectroscopy as a function of the relative molar ratios of oligopeptide and metal complex. Representative examples of the change in the UV−visible absorbance during these titrations are shown in Figure 2 for each of the metal complexes with pyridine tetramer, **4**. In Figure 2A, the broad peak at 662 nm (associated with a Cu d−d transition) increases in intensity and levels at a constant absorbance value. Analogous spectra are shown for the $[Cu(tpy)]^{2+}$ (Figure 2B) and $[Pt(tpy)]^{2+}$ (Figure 2C) complexes. In each case, the Figure 2 insets show that the absorbance intensities increase and reach a limiting value at a molar ratio of 4 metal complexes:1 oligopeptide. These data indicate that each of the four pyridine ligands on the oligopeptide are capable of binding one metal complex in a stoichiometric fashion.

We have performed similar titrations using each of the oligopeptides in the series **1**, **4**, **5**, **6**, and **10** using the metal complexes $[Cu(tpy)]^{2+}$, $[Pt(tpy)]^{2+}$, and [Cu(pda)]. Titrations of oligopeptides **4**, **5**, **6**, and **10** with [Pt(pda)] resulted in precipitation from solution, even with solvents such as DMF and dimethyl sulfoxide (which readily dissolve the other metalated oligopeptides), precluding collection of the UV−visible titration data. The equivalence points for the reaction of each of the oligopeptides and metal salts were determined from the titration curves by least-squares fitting of the data and are listed in Table 2.

The empirical equivalence points agree well with the predicted stoichiometries for the metal complex ligation of the pyridine substituents. Even the longest oligopeptides are able to bind stoichiometric quantities of metals to create large, multinuclear complexes. Importantly, these titration data show that complexation is independent of metal complex charge, since the $[Pt(tpy)]^{2+}$ and $[Cu(tpy)]^{2+}$ dication complexes bind equivalently to the charge-neutral [Cu(pda)] complexes. For the longest oligopeptide, **10**, the total charge for the Pt(II)and Cu(II) tpy complexes is *+20*.

Purity of the titration products was confirmed using ^{1}H NMR (not shown), and while these spectra are broadened (compared to the unmetalated oligomers) by the presence of metals, the spectra of all metal−oligopeptide complexes give the expected integrations for the pure, stoichiometrically complexed oligopeptides. In the case of the Cu(II)-containing molecules, the aromatic pyridyl protons disappear from the low-field region of the spectrum due to the paramagnetic nature of the bound Cu^{2+} metal center. This result also suggests that attachment of the metals occurs at the desired ligand rather than to the peptide backbone (vide infra).

Metal Coordination to Acetyl Tetrapeptides. Metal ions are known to bind weakly to secondary amine and amide groups and carbonyl oxygens,[15] all of which are plentiful on the oligopeptide backbone. To test the specificity of metal

(13) Harris, D. C. *Quantitative Chemical Analysis*, 4th ed.; W. H. Freeman and Co.: New York, 1996.
(14) Vaidya, R. A.; Mathias, L. J. *J. Am. Chem. Soc.* **1986**, *108*, 5514−5520.

Scheme 2. Pyridyl Oligopeptide Coordination to M = Cu(II) or Pt(II) Complexes

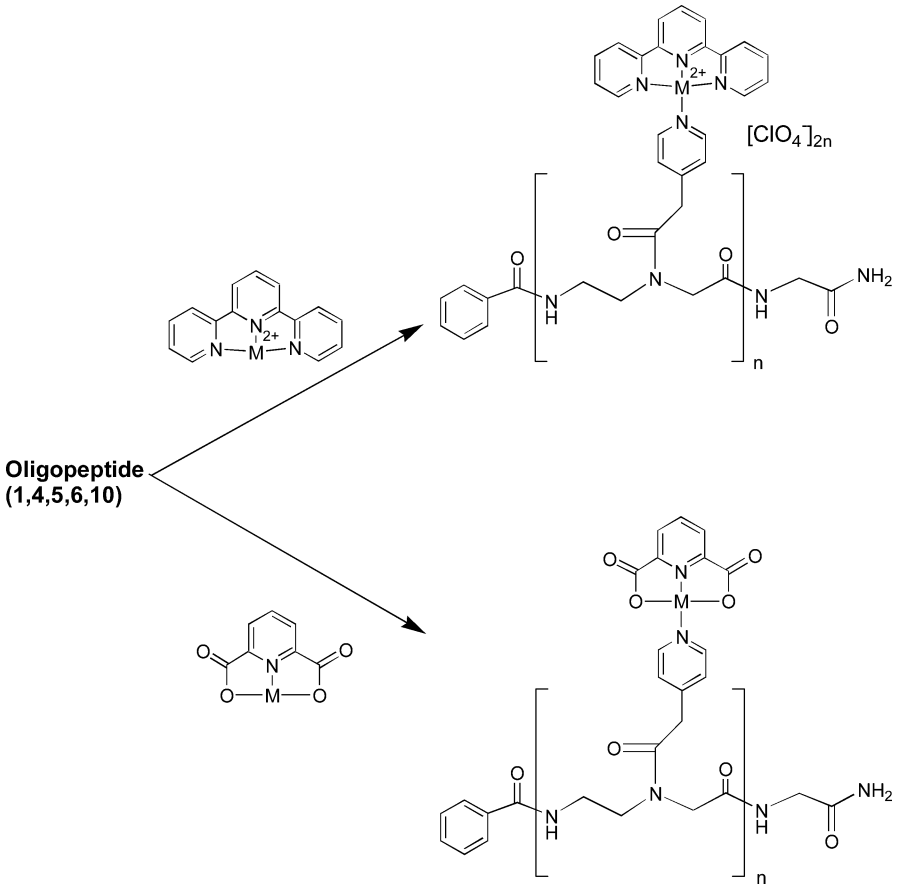

complex coordination with the pyridine ligand sites rather than to these groups on the peptide, we prepared an acetyl-functionalized tetrapeptide, **4Ac** (Scheme 1)**.** The identity and purity of the acetyl tetramer were confirmed with mass spectrometry and ^{1}H NMR spectroscopy. This tetramer is equivalent in length to oligopeptide **4** (above) but contains methyl substituents in place of the pyridine ligands and should not contain any moieties with particularly high affinity for transition metals. To test this, titrations with each of the metal complexes were performed analogously to the experiments with the pyridine oligomers (vide supra). Figure 3 compares titrations of the acetyl and pyridine tetrapeptides. Minor increases in the UV−visible absorption spectra were observed upon reaction with $[Cu(tpy)]^{2+}$, but no observable change was seen for the $[Pt(tpy)]^{2+}$ or [Cu(pda)].

The specific nature of the interaction of $[Cu(tpy)]^{2+}$ with the oligopeptide backbone is not known, however, as the inset of Figure 3B shows, the absorbance change for titration with **4Ac** is far less than that observed for the titration with the pyridine oligomer. The absorbance change associated with backbone interaction is sufficiently minor that it does not affect the stoichiometry of complexation with the pyridine oligomers, which clearly shows a 1:1 ratio for pyridine/$[Cu(tpy)]^{2+}$ bond formation for each length of oligopeptide (Table 2). This is most likely due to a competitive equilibrium between binding the backbone and pyridine ligand (in the pyridine oligopeptides), where bond formation with the pyridine ligand would be thermodynamically favored.

Molecular Modeling. The titration products are isolated as fine powders, and while their purity is confirmed by NMR spectroscopy, we have been unable to grow crystallographic-quality crystals to date. To understand the structures of the oligopeptides, we have turned to molecular modeling. Simple molecular mechanics calculations were performed to obtain the energy-minimized structures of both the protonated pyridine oligopeptides and $[Pt(tpy)]^{2+}$-coordinated structures; the latter of these are shown in Figure 4 for the series **1**, **4**, **5**, **6**, and **10**. Note that charge-compensating counteranions are not shown in these structures but would contribute to their overall hydrodynamic size.

(15) (a) Kowalik-Jankowska, T.; Rajewska, A.; Szeszel-Fedorowicz, W. *Polyhedron* **2005**, *24*, 443−450. (b) Shields, B. S.; Franklin, S. J. *Biochem.* **2004**, *43*, 16086−16091. (c) Jakusch, T.; Dornyei, A.; Correia, I.; Rodriques, L. M.; Toth, G. K.; Kiss, T.; Pessoa, J. C.; Marcao, S. *Eur. J. Inog. Chem.* **2003**, *11*, 2113-2122. (d) Pessoa, J. C.; Correia, I.; Kiss, T.; Jakusch, T.; Castro, M. M.; Geraldes, C. F. *J. Chem. Soc., Dalton Trans.* **2002**, *23*, 4440−4450. (e) Garcia-Roso, A.; Fiol, J. J.; Adrover, B.; Caubet, A.; Espinosa, E.; Mata, I.; Molins, E. *Polyhedron* **2002**, *21*, 1197−1201. (f) Santra, B. K.; Reddy, P. A.; Nethaji, M.; Chakravarty, A. R. *J. Chem. Soc., Dalton Trans*. **2001**, *24*, 3553−3555. (g) Runganathan, S.; Tamilarasu, N. *Inorg. Chem.* **1999**, *38*, 1019−1023. (h) Holtz, R. C.; Bennett, B.; Chen, G.; Ming, L. *J. Am. Chem. Soc.* **1998**, *120*, 6329−6335.

(16) (a) Wong, K. M.; Tang, W.; Chu, B. W.; Zhu, N.; Yam, V. W. *Organometallics* **2004**, *23*, 3459−3465. (b) Yam, V. W.; Hui, C.; Yu, S.; Zhu, N. *Inorg. Chem.* **2004**, *43*, 812−821. (c) Rakhimov, R. D.; Weinstein, Y. A.; Lileeva, E. V.; Zheligovskaya, N. N.; Mel'nikov, M. Y.; Butin, K. P. *Russ. Chem. Bull.* **2003**, *52*, 1150−1156. (d) Moore, J. J.; Nash, J. J.; Fanwick, P. E.; McMillin, P. R. *Inorg. Chem.* **2002**, *41*, 6387−6396. (e) Yang, L.; Wimmer, F. L.; Wimmer, S.; Zhao, J.; Braterman, P. S. *J. Organomet. Chem.* **1996**, *525*, 1−8.

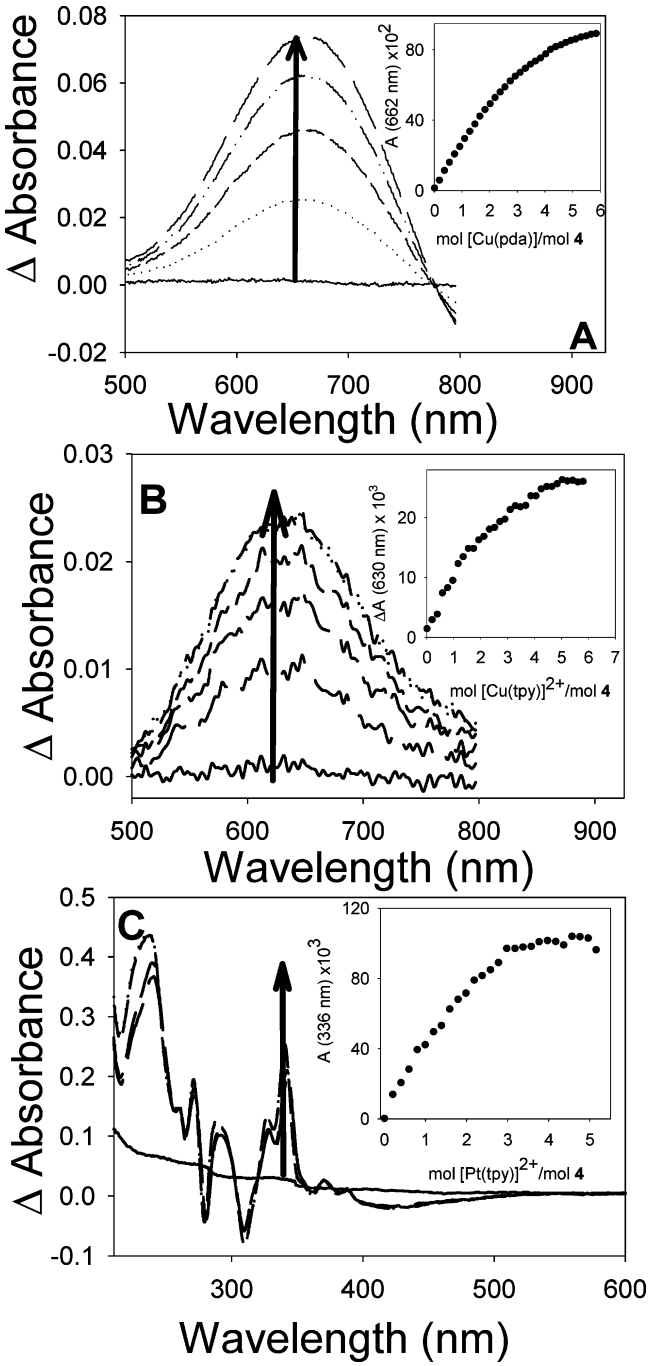

Figure 2. UV−visible absorption spectra acquired during the reaction of pyridine tetramer (**4**) with metal complexes: (A) 3.875 mM peptide (**4**) with 3.25 mM [Cu(pda)] in MeOH; (B) 2.09 mM peptide (**4**) with 29.9 μM $[Cu(tpy)]^{2+}$ in 2.5% H_2O in MeOH; and (C) 0.124 mM peptide (**4**) with 99.9 μM $[Pt(tpy)]^{2+}$ in 25% H_2O in MeOH. The insets of each plot show the increases in absorbance at 662, 630, and 336 nm for A, B, and C, respectively.

The calculated structures reveal that, despite favorable $\pi-\pi$ interactions of the aromatic ligands, electrostatic repulsions between the $[Pt(tpy)]^{2+}$ complexes push these apart to distances of ~1.5 nm. While the models have linearly extended structures of increasing length as the number of pyridyl units increase, the peptide backbone is expected to be highly flexible in solution, allowing for conformationally dynamic structures. We do not expect or observe any tertiary structures, analogous to biomolecular systems, for these relatively short-chain peptides. The models in Figure 4 indicate that the long axis of the multimetallic peptides increases by a factor of ~7 from compound **1** to **10** in the series.

Table 2. Stoichiometry of Metal Complexation with the Oligopeptides

	stoichiometric equivalent of metal complex (mol complex/mol oligopeptide)		
oligopeptide	[Cu(pda)]	$[Cu(tpy)]^{2+}$	$[Pt(tpy)]^{2+}$
1	0.9 ± 0.1	1.0 ± 0.1	1.1 ± 0.1
4	4.2 ± 0.2	4.2 ± 0.2	3.6 ± 0.3
5	5.3 ± 0.2	4.5 ± 0.2	4.6 ± 0.2
6	5.9 ± 0.1	6.0 ± 0.1	5.4 ± 0.2
10	9.8 ± 0.2	10.3 ± 0.2	9.9 ± 0.2

Electrochemistry. While the electrochemical characterization of the Cu(II)-complexed oligopeptides was precluded by apparent adsorption and electrochemical irreversibility (see Supporting Information), the cyclic voltammetry of each of the $[Pt(tpy)]^{2+}$-decorated oligopeptides **1**, **4**, **5**, **6**, and **10** contains two sequential reduction waves at formal potentials of −0.6 and −1.1 V vs SCE. Representative cyclic and differential pulse voltammograms are shown in Figure 5 for the complexes $[(Pt(tpy))(\mathbf{1})]^{2+}$ and $[(Pt(tpy))(\mathbf{5})]^{10+}$. On the basis of reported voltammetry for the small-molecule analogue $[Pt(tpy)(py)](PF_6)_2$, these reactions are tpy-centered reductions (with some possible mixing of Pt character);[16,17] the formal potentials are given in Table 3 for each of the complexes. For the series of metalated oligopeptides, the peak currents for the cathodic and anodic reactions are equivalent, indicating that the two reactions are chemically reversible. It is noteworthy that there is no evidence for adsorption to the electrode surface for even the largest oligopeptide, which undergoes a change in charge from +20 to neutral upon reaction with 20 electrons. In all cases, the average difference between peak potentials (ΔE_p) is ~75 mV, and neither E° nor ΔE_p were found to be dependent on oligopeptide length (Table 3). Together, these data lead to the conclusion that the attached $[Pt(tpy)]^{2+}$ redox centers are electronically isolated and behave independently; that is, each of the two reactions are electrochemically quasi-reversible, one-electron reductions. While these data are in contrast to the observation of the trend in pK_A for the unmetalated pyridine oligopeptides, they imply that the greater charge of the Pt complexes creates electrostatic repulsions that push the dicationic redox centers to distances that would prevent electronic communication, consistent with the calculated molecular models in Figure 4.

Since the redox centers are apparently reacting with the electrode surface independently (i.e., $n = 1$ reactions), it is expected that the amount of observed current should increase as the peptide chain length and attached $[Pt(tpy)]^{2+}$ increases. In Figure 6, the cyclic voltammograms of the metalated complexes of oligopeptides **4**, **6**, and **10** obtained at the same potential scan rate (50 mV/s) are normalized[18] for the concentration of $[Pt(tpy)]^{2+}$ and overlaid. The relative amount of current observed during the voltammetry *decreases* with

(17) Hill, M. G.; Bailey, J. A.; Miskowski, V. M.; Gray, H. B. *Inorg. Chem.* **1996**, *35*, 4585−4590.

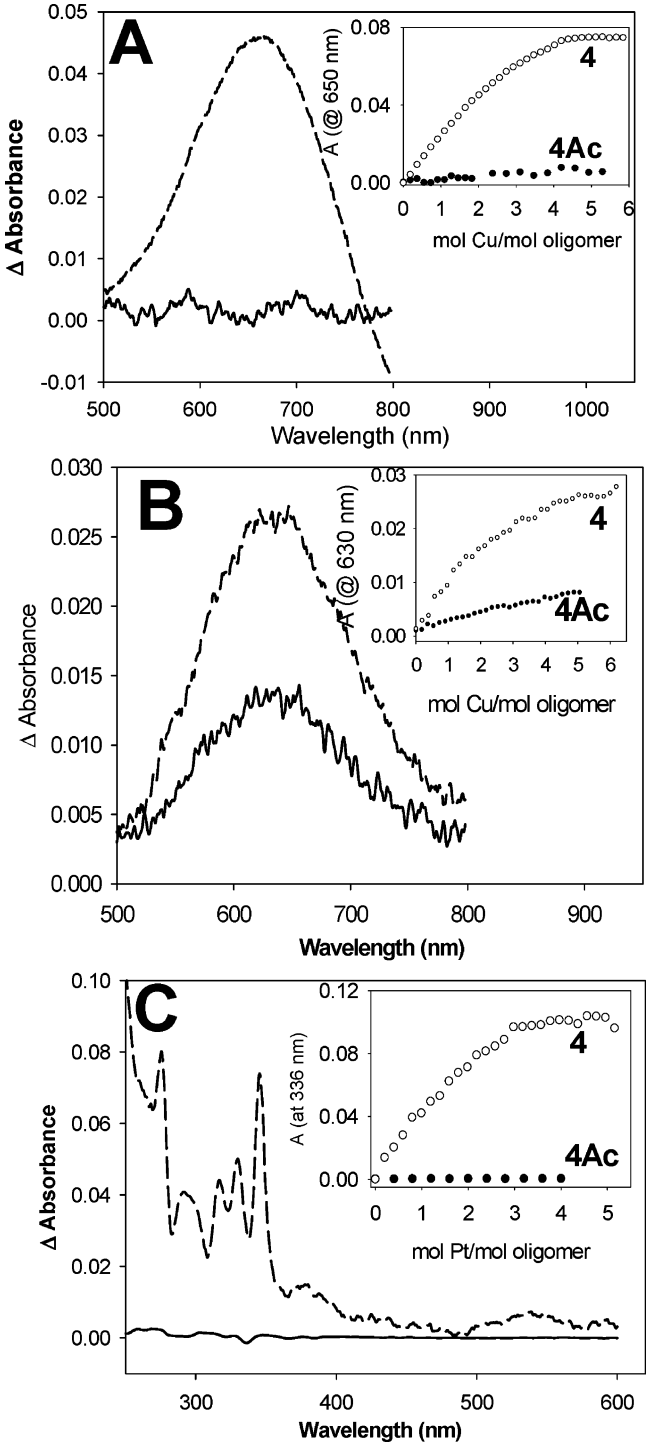

Figure 3. Change in UV−visible absorption spectra during the titration of acetyl tetramer, (**4Ac**, −) and py tetramer (**4**, − − −) with metal complexes: (A) 4.0 mM peptide **4Ac** with 3.25 mM [Cu(pda)in MeOH; (B) 2.1 mM peptide **4Ac** and 29.9 μM [Cu(tpy)]$^{2+}$ in 2.5% H_2O in MeOH; and (C) 0.13 mM peptide **4Ac** with 99.9 μM [Pt(tpy)]$^{2+}$ in 25% H_2O in MeOH. The insets compare the change in absorbance for **4Ac** (●) and **4** (○) at the indicated wavelengths.

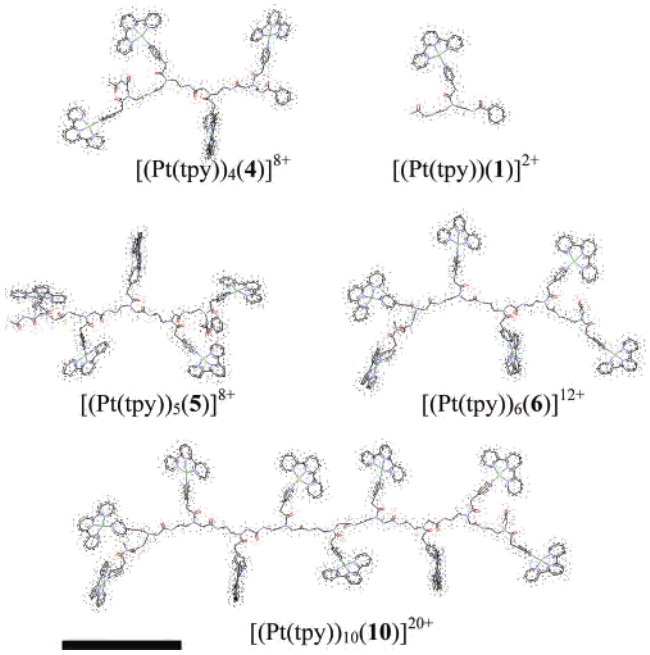

Figure 4. Energy-minimized structures of [Pt(tpy)]$^{2+}$-coordinated series of pyridine oligopeptides, with the H atoms omitted for clarity. Scale bar is 2 nm.

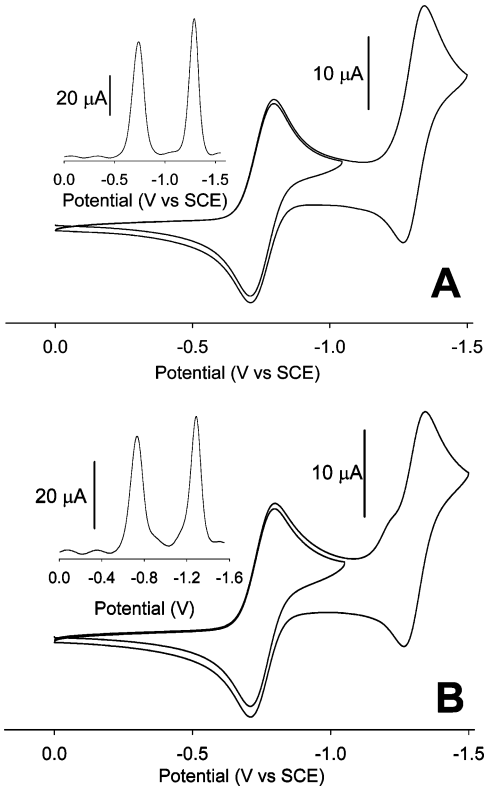

Figure 5. Cyclic voltammograms of (A) 1.35 mM [Pt(tpy)(**1**)]$^{2+}$ and (B) 0.258 mM [(Pt(tpy))$_5$(**5**)]$^{10+}$ solutions containing 0.2 M TBAP in DMF, using a glassy carbon working electrode and potential scan rate of 50 mV/s. Insets contain reductive scan differential pulse voltammograms.

the size of the multimetallic oligopeptides. To understand this, plots such as that shown in the Figure 6 inset examine the relationship between cathodic peak current (i_p) of the first reduction reaction as a function of scan rate. For an electrochemically reversible reaction, these are related by the equation:[7]

$$i_p = 2.69 \times 10^5 n^{3/2} A D^{1/2} C v^{1/2} \quad (1)$$

(18) The concentration of [Pt(tpy)]$^{2+}$ is taken as the known concentration of oligopeptide multiplied by the number of attached Pt complexes.

Table 3. Electrochemical Data for Pyridine Oligopeptides with Bound $[Pt(tpy)]^{2+}$

compound		$[Pt(tpy)]^{2+/1+}$		$[Pt(tpy)]^{1+/0}$			
oligomer	# of $[Pt(tpy)]^{2+}$	$E°$ (V)[a]	ΔE_p (mV)[b]	$E°$ (V)[a]	ΔE_p (mV)[b]	$\Delta E°$ (V)[c]	$D \times 10^6$ (cm^2/s)[d]
1	1	−0.59	74	−1.14	74	0.55	11 ± 1
4	4	−0.58	85	−1.13	74	0.55	8 ± 1
5	5	−0.60	80	−1.14	72	0.54	9 ± 1
6	6	−0.60	83	−1.14	68	0.55	6.2 ± 0.8
10	10	−0.57	67	−1.13	84	0.56	1.2 ± 0.4

[a] Formal potential measured as the average peak potential for the reaction in V vs SCE, measured using a potential scan rate of 50 mV/s. [b] Difference in the cathodic and anodic peak potentials in the cyclic voltammogram, measured at a potential scan rate of 50 mV/s. [c] Separation between the first and second reduction reactions, measured as the difference in formal potential. [d] Calculated from the slopes of the Cottrell plots from chronoamperometry (Figure 7) and analyzed using eq 2.

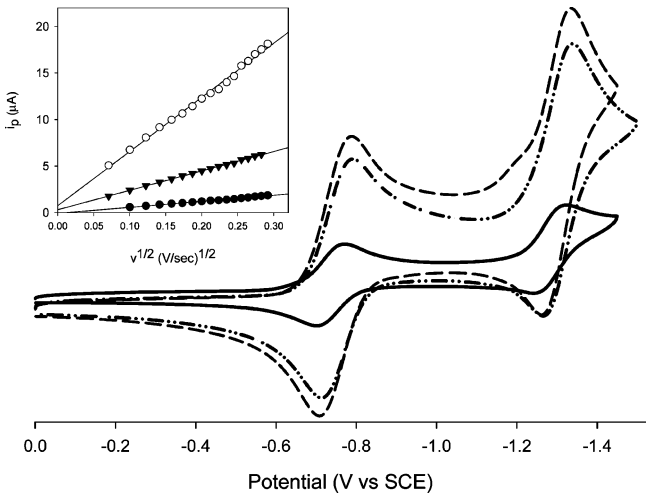

Figure 6. Cyclic voltammograms of the metalated oligopeptides $[(Pt(tpy))_4(\mathbf{4})]^{8+}$ (−); $[(Pt(tpy))_6(\mathbf{6})]^{12+}$ (− ·· −); and $[(Pt(tpy))_{10}(\mathbf{10})]^{20+}$ (− − −), normalized for the concentration of $[Pt(tpy)]^{2+}$, in solutions containing 0.2 M TBAP in DMF. Potential scan rates were 50 mV/s. Inset is plots of the peak cathodic currents versus the square root of the scan rate for **4** (○), **6** (▼), and **10** (●) with bound $[Pt(tpy)]^{2+}$.

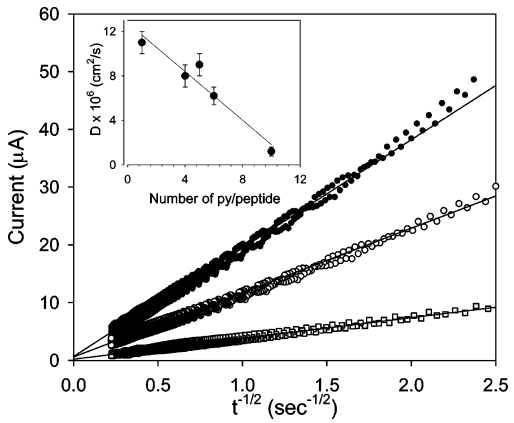

Figure 7. Linearized current−time transients resulting from an applied potential step of −1.0 V for the metalated oligopeptides $[Pt(tpy)(1)]^{2+}$ (●), $[(Pt(tpy))_5(\mathbf{5})]^{10+}$ (○), and $[(Pt(tpy))_{10}(\mathbf{10})]^{20+}$ (□), with linear regressions. Inset: Plot of the measured diffusion coefficient vs the number of pyridine ligands per oligopeptide, with a line to guide the eye.

where n is one electron; A is the surface area of the working electrode (cm^2); C is the concentration of the reactant (mol/cm^3); D is the diffusion coefficient (cm^2/s); and ν is the potential scan rate (V/s). On the basis of the linearity of the plots in the Figure 6 inset, the reduction reactions are diffusion controlled.

However, because the reactions are quasi-reversible, the use of eq 1 to evaluate the slopes in Figure 6 ultimately underestimates D, and we instead use potential step chronoamperometry to analyze the mass transport rate of each of the $[Pt(tpy)]^{2+}$-metalated oligomers. Figure 7 shows the linearized current−time transients that are the result of application of a large overpotential to the mass-transport-limited region of the first reduction wave (−1.0V) for the $[Pt(tpy)]^{2+}$-complexed **1**, **5**, and **10** oligopeptides. The linearity of these plots is again indicative of diffusion-controlled reactions. These data were used to calculate the diffusion coefficients of each molecule by use of the Cottrell equation[7]

$$i = \frac{nFAD^{1/2}C}{\pi^{1/2}t^{1/2}} \tag{2}$$

using the known concentration of $[Pt(tpy)]^{2+}$ in each oligopeptide sample, and are listed in Table 3. As shown in the Figure 7 inset, the measured diffusion coefficients decrease as the number of pyridine ligands (i.e., length) on the oligomer increases. This relationship is expected, since the mass transport of molecules is inversely proportional to their size and is described by the Stokes−Einstein equation:[19]

$$D = \frac{k_B T}{6\pi\eta a} \tag{3}$$

where k_B is Boltzman's constant; T is the absolute temperature; η is the solution viscosity; and a is the hydrodynamic radius of the molecule. It is evident from the molecular modeling that the length of the molecule increases by ~7-fold; the electrochemical data show that, over the same series of molecules, the calculated D decreases by an order of magnitude, so that there is a slight deviation from the relationship described by eq 3. This could arise from the large number of counteranions and solvent molecules that diffuse with the metalated oligopeptides and contribute to their overall hydrodynamic radii but is most likely a result of the roughly cylindrical molecular shape of these multimetallic structures.

Conclusion. We have presented the facile construction of a series of supramolecular structures containing multiple and variable metal complexes tethered to pyridine-substituted oligopeptide scaffolds. These self-assembled structures may

(19) Atkins, P.; de Paula, J. *Physical Chemistry*, 7th ed.; W. H. Freeman and Company: New York, 2002.

provide new strategies for chelation-based molecular recognition, and their unique optical and electronic properties could find utility in biomolecular recognition.

Acknowledgment. We are grateful to the David and Lucile Packard Foundation for generous support of this work through a Science and Engineering Fellowship. K.O. acknowledges support as a Penn State University Robert's Graduate Fellow. We thank C. M. Morgan for assistance with figure production.

Supporting Information Available: Electrochemical and NMR data for selected pure and metalated peptides. This material is available free of charge via the Internet at http://pubs.acs.org.

IC050769I